THE GEOLOGICAL SOCIETY OF AMERICA®

# A new interpretation for the nature and significance of mirror-like surfaces in experimental carbonate-hosted seismic faults

Giacomo Pozzi[1], Nicola De Paola[1], Stefan B. Nielsen[1], Robert E. Holdsworth[1], and Leon Bowen[2]
[1]Department of Earth Sciences, Rock Mechanics Laboratory, Durham University, Durham, DH1 3LE, UK
[2]Department of Physics, Durham University, Durham, DH1 3LE, UK

## ABSTRACT

**Highly reflective, continuous smooth surfaces, known as "mirror-like surfaces" (MSs), have been observed in experimental carbonate-hosted faults, which were sheared at both seismic and aseismic velocities. MSs produced during high-velocity friction experiments (>0.1 m s$^{-1}$) are typically interpreted to be frictional principal slip surfaces, where weakening mechanisms are activated by shear heating. We re-examined this model by performing friction experiments in a rotary shear apparatus on calcite gouge, at seismic velocities up to $v$ = 1.4 m s$^{-1}$ and normal stress $\sigma_n$ = 25 MPa, to analyze the evolution of microstructures as displacement increases. After the onset of dynamic weakening, when the friction coefficients are low ($\mu \ll 0.6$), sheared gouges consistently develop a well-defined, porosity-free principal slip zone (PSZ) of constant finite thickness (a few tens of micrometers) composed of nanometric material, which displays polygonal grain shapes. MSs occur at both boundaries of the PSZ, where they mark a sharp contrast in grain size with the sintered, much coarser material on either side of the PSZ. Our observations suggest that, with the onset of dynamic weakening, MSs partition the deformation by separating strong, sintered wall rocks from a central weak, actively deforming viscous PSZ. Therefore, the MSs do not correspond to frictional slip surfaces in the classical sense, but constitute sharp rheological boundaries, while, in the PSZ, shear is enhanced by thermal and grain-size–dependent mechanisms.**

## INTRODUCTION

Highly reflective smooth surfaces, known as "mirror-like surfaces" (MSs), have long been found and described along natural exhumed faults. More recently, it has been proposed that they may represent a possible microstructural proxy for past seismic activity in carbonate-hosted fault zones (Siman-Tov et al., 2013). Several authors have since demonstrated that continuous MSs develop in carbonate gouges and rocks when sheared at seismic velocities (> 0.1 m s$^{-1}$)—in situations where frictional weakening is also observed—and have proposed different interpretations of their role in the weakening process (e.g., Smith et al., 2013, 2015; Siman-Tov et al., 2015; Green et al., 2015; De Paola et al., 2015). Other authors, however, have produced patchy MSs during lower-velocity experiments (0.1–10 µm s$^{-1}$), and therefore questioned their reliability as seismic markers (e.g., Verberne et al., 2013).

When dynamic fault weakening is observed, MSs are typically interpreted to be principal slip surfaces developed within and/or at the boundary of a slip zone. It has been argued that weakening during shear along the MSs can be driven by flash heating (Smith et al., 2015) or by thermal runaway at dynamic asperities (Siman-Tov et al., 2015). In support of these models, there is also evidence of temperature-activated crystal plasticity in the immediately adjacent rock volumes. Other authors have suggested that grain-size–sensitive creep mechanisms, occurring in a narrow (<100-µm-thick), ultrafine-grained shear zone, can cause coseismic weakening (Green et al., 2015; De Paola et al., 2015). However, the role played by MSs throughout the weakening history of carbonate gouges is still uncertain, as is the partitioning of strain between presumed sliding along MSs and bulk deformation by grain boundary sliding and/or crystal plasticity within the main slip zone.

Here, we integrate mechanical data and microstructural observations to develop a new conceptual model concerning the role and significance of MSs throughout the weakening history of calcite gouges sheared at seismic velocities.

## MECHANICAL DATA

We performed friction experiments on simulated calcite gouge (grain size: 63–90 µm) in a low- to high-velocity rotary shear apparatus (De Paola et al., 2015). A sample assembly with two hollow cylinders made of a titanium-vanadium alloy (Ti-alloy, Ti90Al6V4; Yao et al., 2016) was used to sandwich a layer of gouge (weight of 1 g and initial thickness ~1.4 mm), which was confined using a Teflon outer ring and an inner Teflon cylinder (see Section DR1 in the GSA Data Repository[1]). All experiments were run at room temperature and humidity conditions; normal stress, $\sigma_n$, of ~25 MPa; and slip rates up to $v$ = 1.4 m s$^{-1}$ calculated at the reference radius of ~8.9 mm. Experiments were arrested at different displacements (up to 1 m, for a duration <1 s) to analyze the evolution of microstructures of samples throughout their weakening path.

Dynamic weakening was observed in experiments run at $v$ > 0.1 m s$^{-1}$, in good agreement with values typical of seismic slip rates (Smith et al., 2013). The evolution of strength of the experimental fault follows a characteristic weakening profile characterized by four distinct phases (Fig. 1; axial shortening data are reported in Section DR3). During Stage I, Byerlee's friction values of µ > 0.6 were attained, and slip-hardening up to peak values of µ = 0.9 is observed (Fig. 1). Experiments consistently showed the onset of weakening after an amount of slip of δ ~6.4 cm and δ ~4.7 cm for target velocities of $v$ = 0.14 m

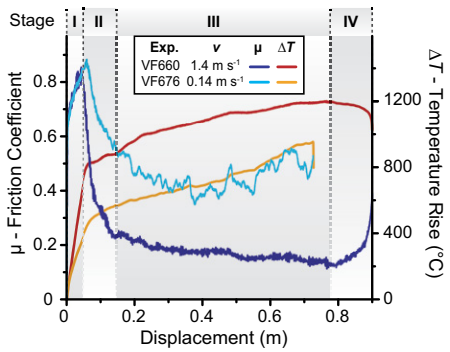


**Figure 1. Mechanical data for two representative experiments (Exp.; $v$ = 1.4 and $v$ = 0.14 m s$^{-1}$): friction coefficient (µ, shown in cold colors [blues]) and estimated temperature rise (Δ$T$, shown in warm colors [orange, red]) curves are plotted versus displacement. The four stages of friction evolution are highlighted by the shaded areas.**

[1]GSA Data Repository item 2018194, Sections DR1 (Sample assembly), DR2 (temperature estimate), DR3 (mechanical data), DR4 (flow laws), and DR5 (microstructures), is available online at http://www.geosociety.org/datarepository/2018/ or on request from editing@geosociety.org.

$s^{-1}$ and $v \geq 0.25$ m $s^{-1}$, respectively (Stages I and II in Fig. 1). During Stage II, the material weakens in an exponential fashion to low, rate-dependent friction values, $\mu = 0.5–0.4$ at $v = 0.14$ m $s^{-1}$ and $\mu = 0.2–0.15$ at $v = 1.4$ m $s^{-1}$, which then remain low throughout Stage III (Fig. 1). During Stage IV, material strengthens up to friction values $\mu = 0.4–0.5$ upon deceleration of the motor to arrest (Fig. 1).

We use a simple mono-dimensional thermal diffusion model (Rice, 2006) to calculate the bulk temperature rise associated with the development of a thin slip zone (Section DR2). Due to the high angular strains ($\gamma >> 10$) and strain rates ($\dot{\gamma} > 10^3$) attained during the experiments, it is reasonable to assume that, to a first approximation, all of the deformation energy in the deforming slip zone is dissipated as heat (Hobbs and Ord, 2014, and references therein). The estimated temperature at the onset of weakening, $T_w$ (beginning of Stage II) is rate-dependent, with $T_w$ ~470 °C and $T_w$ ~750 °C for $v = 0.14$ m $s^{-1}$ and $v = 1.4$ m $s^{-1}$, respectively. Repeated runs show a consistent evolution in the mechanical data, proving good reproducibility of the experimental results (Section DR3).

## MICROSTRUCTURAL OBSERVATIONS

After the experiments, sample chips were carefully removed from the rotary assembly and embedded in epoxy to preserve the whole thickness of the gouge layer (Fig. 2). We used a FEI Helios Nanolab 600 electron microscope to acquire backscattered and forescattered electron images on polished cross sections, which were cut parallel to the slip direction and perpendicular to the gouge layer boundaries, at the reference radius (~8.9 mm). The values of grain size and slip zone thickness reported here refer to samples sheared at $v = 1.4$ m $s^{-1}$.

Gouge samples recovered at the end of Stage I are porous, slightly cohesive, and show the effect of widespread brittle grain-size reduction (Fig. 2A). During this stage, deformation is mostly accommodated by Riedel shears (R and R′) and is within an ~100-μm-thick Y-shear zone (Fig. 2A), where extreme grain-size reduction occurs (down to a few tens of nanometers). Microstructures change during Stage II, from the onset of weakening, when the Y-shear zone evolves to a well-defined principal slip zone (PSZ) with sharp boundaries and inhomogeneous grain size, with larger clasts (<1 μm) dispersed within a finer-grained matrix (mean grain size ~100 nm; Figs. 2B and 2C). Volumes of low-porosity sintered material, with thicknesses of ~20 μm, form outside the PSZ (Fig. 2C) and their surfaces bound the PSZ, forming discontinuous MSs.

At the end of the transient stage of decay from peak to low friction values (Stage II) and throughout Stage III, the PSZ becomes a discrete, porosity-free volume of fine, polygonally recrystallized material with constant thickness (~30 μm; Figs 2D, 3A, and 3B). The internal structure of the PSZ shows fairly homogeneous grain size, triple junctions, and oblique foliation, marked by a shape-preferred orientation of the crystals, consistent with the overall (sinistral) sense of shear (Fig. 3B; Section DR5, Fig. DR17). This texture is similar to that observed in some natural (Bestmann et al., 2000; Herwegh and Kunze, 2002) and experimental (Barnhoorn et al., 2004) calcite ultramylonites.

PSZ grain size increases from an average of ~300 nm at the beginning of Stage III to ~700 nm (Fig. 3B) after ~0.75 m of slip (Section DR5, Fig. DR17). The texture observed in proximity to, but outside, the PSZ is similar to that observed inside the PSZ, but shows an abrupt increase in grain size of approximately one order of magnitude (>1 μm; Fig. 3B). Such marked grain-size decoupling produces sharp planar boundaries on either side of the PSZ: the MSs (Fig. 3B; Section DR5, Fig. DR7). In the outer layers, away from and on both sides of the PSZ, porosity gradually increases as recrystallization becomes less pervasive, forming what we term here a 'sintering gradient' (SG; Fig. 2D). In these regions, an array of relict subparallel MSs is observed (white lines in Fig. 3A). The younger MSs are straight and smooth, and show a homogeneous grain size along them (Figs. 3A and 3B). Another set of more irregular MSs is also observed (Fig. 3A), and interpreted to represent older MSs due to their similarity to the patchy ones formed during the early Stage II (Fig. 2C). These are locally reworked and may truncate larger clasts (e.g., Fondriest et al., 2013) during formation and localization of the early PSZ.

During Stage IV, brittle dilatant fracturing occurs and appears to be consistently restricted to the PSZ (e.g., Fig. 2E). It includes splitting along the MSs (exploited by epoxy during sample preparation; Fig. 3B), which exposes shiny MSs visible in recovered samples (Section DR5, Fig. DR7A). These structures always unavoidably overprint—but do not obliterate—microstructures developed during Stage III.

Similar to findings discussed by De Paola et al. (2015), our microstructural and mineralogical observations revealed that, during Stage III and IV, the PSZ is composed of crystalline calcite. This confirms that decarbonation reactions were not quantitatively significant during our experiments.

## DISCUSSION

With its finite volume, parallel boundaries, and textural decoupling with the outer layers, we

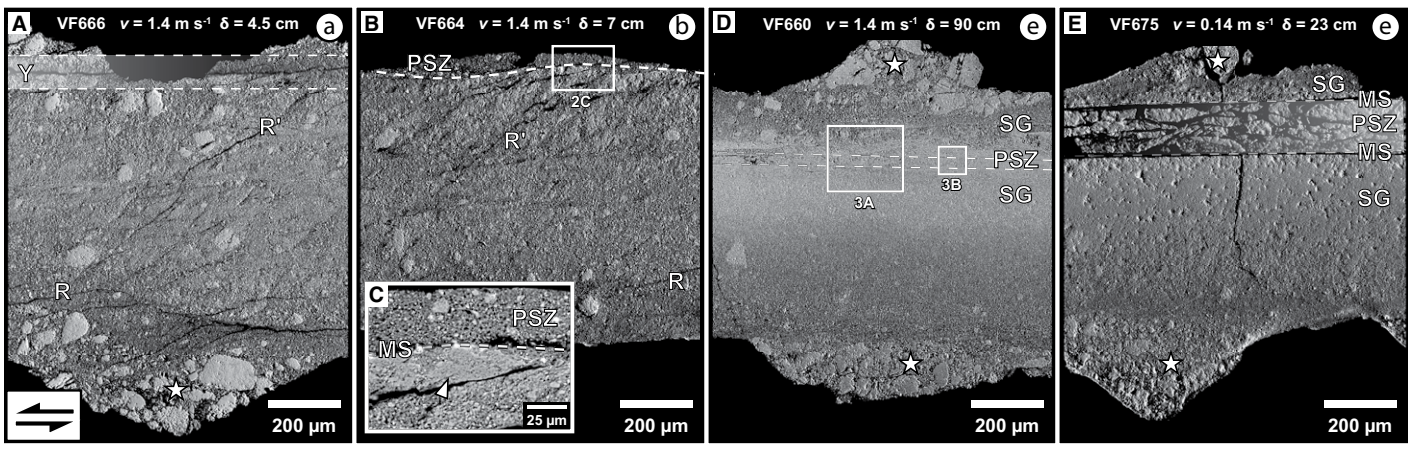


**Figure 2. Backscattered electron images of sample cross sections obtained from the whole thickness of gouge layer (see the coarse-grained gouges filling the grooves machined on the top and bottom sample assembly cylinders, indicated with white stars) cut at the reference radius. Shear sense is sinistral. A: Stage I: diffuse and localized deformation with Riedel shear bands (R, R′) and a horizontal Y shear band (Y). B: Stage II: well-developed principal slip zone (PSZ) with patchy recrystallized boundary ("mirror-like surface", MS). C: Close-up of area outlined in B. D,E: Stages III and IV: fully developed PSZ bounded by MSs and sintered deactivated layers (sintering gradient, SG) of experiments run at $v = 1.4$ m $s^{-1}$ and $v = 0.14$ m $s^{-1}$, respectively. Stage IV damage in the PSZ is more evident in the lower-velocity experiment. Lowercase letters link to microstructural sketches shown in Figure 4A.**

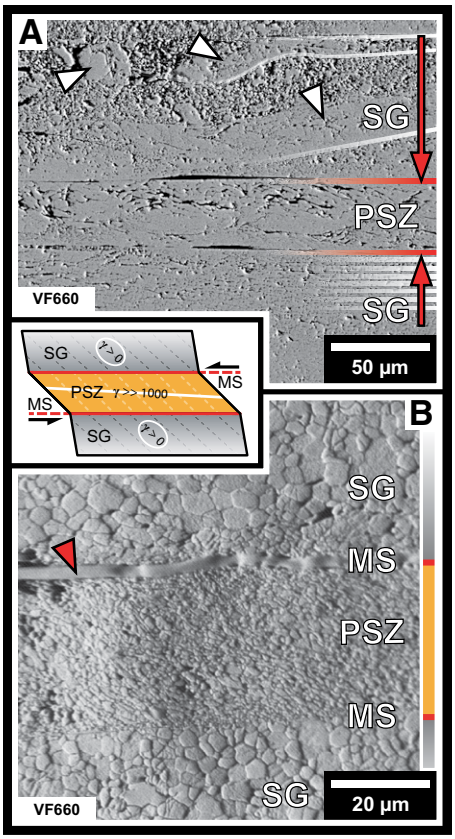


**Figure 3. Close-up scanning electron microscopy images of Stages III and IV principal slip zone (PSZ) cross sections (same sample as in Fig. 2D, *v* = 1.4 m s$^{-1}$, δ = 90 cm). A: Backscattered electron image showing relict (highlighted with white lines) and the last active (red lines) "mirror-like surfaces" (MSs); white arrows indicate the older, irregular, reworked MSs; red arrows indicate direction of migration of the PSZ boundaries during localization. SG—sintering gradient. B: Forescattered electron image of PSZ displaying oblique foliation, sharp grain-size transition at the boundaries, and MSs locally split and filled with epoxy during sample preparation (red arrow). Textures inside and outside the PSZ are clearly asymmetric with respect to MSs. In the inset, a schematic model of simple shear is compared to the microstructures. γ—angular strain.**

can reasonably assume that the PSZ corresponds to a zone of finite simple shear strain (inset of Fig. 3), where grain-size–sensitive processes are active (e.g., De Paola et al., 2015; Green et al., 2015). We define $W_{PSZ}$ as the thickness of the PSZ, evolving throughout every stage of the weakening path. $W_{PSZ}$ is constrained by microstructural observations (Figs. 2 and 3). We propose a conceptual model where $W_{PSZ}$ is compared to a theoretical thickness $W_T$ (Fig. 4B). $W_T$ is here defined as the minimum thickness, for a given velocity ($W_T = v/(2\dot{\gamma}_{max})$where $\dot{\gamma}_{max}$ is the maximum strain rate), of an ideal viscous shear zone deforming by grain-size–sensitive creep. $W_T$ is therefore a function of grain size ($D$), temperature ($T$) and shear stress (τ), i.e., $W_T = f(D, T^{-1}, \tau^{-1})$(Poirier, 1985).

During Stage I, brittle deformation, which is initially distributed within the entire gouge-layer thickness, localizes after a small amount of slip into a Y shear band (Figs. 2A and 4B). With increasing displacement, this band becomes a well-defined discrete PSZ, where extreme comminution (D << 1 μm) and increasing bulk temperature occur. Nanometric particles are formed in the PSZ, possibly by shock-like stress release processes (Sammis and Ben-Zion, 2008; Spagnuolo et al., 2015) and brittle failure aided by intragranular crystal plasticity (Siman-Tov et al., 2013; De Paola et al., 2015). At this stage, the PSZ temperature is still relatively low (Fig. 4C) and, consequently, $W_T >> W_{PSZ}$ (Fig. 4B), which means that the dominant strain rate is still controlled by brittle processes (e.g., Smith et al., 2015).

At the beginning of Stage II, as the temperature rises, we infer that the viscous strain rate increases and begins to compete with the brittle one, leading to a rapid decay in friction to the low friction values of Stage III (Figs. 4B and 4C). During Stage II, the PSZ grain size homogenizes and porosity reduces due to plastic yielding of nanograins. The heat diffusing from the PSZ boundaries promotes grain-size growth in the outer regions on either side of the PSZ. During this stage, the PSZ becomes confined between two sharp sintered boundaries, and its thickness reduces as the temperature rises (migration of MSs; see below). When $W_T = W_{PSZ}$, the viscous strain rate becomes dominant, and at this point, the grain-size–sensitive creep controls the strength of the fault (Fig. 4B). The increase in temperature due to viscous shear heating will decrease $W_T$ and can lead to further localization of the PSZ (Fig. 4B), before the achievement of the low friction values of Stage III. As the PSZ narrows, the old boundaries are deactivated and are preserved as closely spaced planar discontinuities (relict MSs) in the coarse-grained sintered layer (Fig. 3A). A similar microstructure has also been observed in natural faults (Tesei et al., 2013; Collettini et al., 2014).

By Stage III, the PSZ has reached steady-state thickness and strain rate, with low, slowly evolving shear stress (viscosity) and grain size (Fig. 4B). We interpret that the oblique foliation formed in the PSZ during Stage III is a steady-state foliation, achieved through cycles of passive rotation and resetting through dynamic recrystallization (e.g., Barnhoorn et al., 2004, and references therein). Thus, it does not reflect the total strain in the PSZ. Following the method of De Paola et al. (2015), a good agreement is found between the shear stresses measured during Stage III and those calculated using existing flow laws for grain-size–sensitive grain boundary sliding in calcite (Section DR4, Fig. DR6).

We propose that throughout Stages II and III, heat produced by shear heating within the PSZ diffuses into regions immediately adjacent to and outside the PSZ, where the strain rate is lower. The dissipated heat leads to the development of sintering gradients (SGs) by quasi-static grain growth and densification in the materials outside the PSZ. At the same time, viscous deformation maintains a homogeneous, nanometric grain size inside the PSZ. These interpretations are supported by our microstructural observations showing a sharp textural contrast

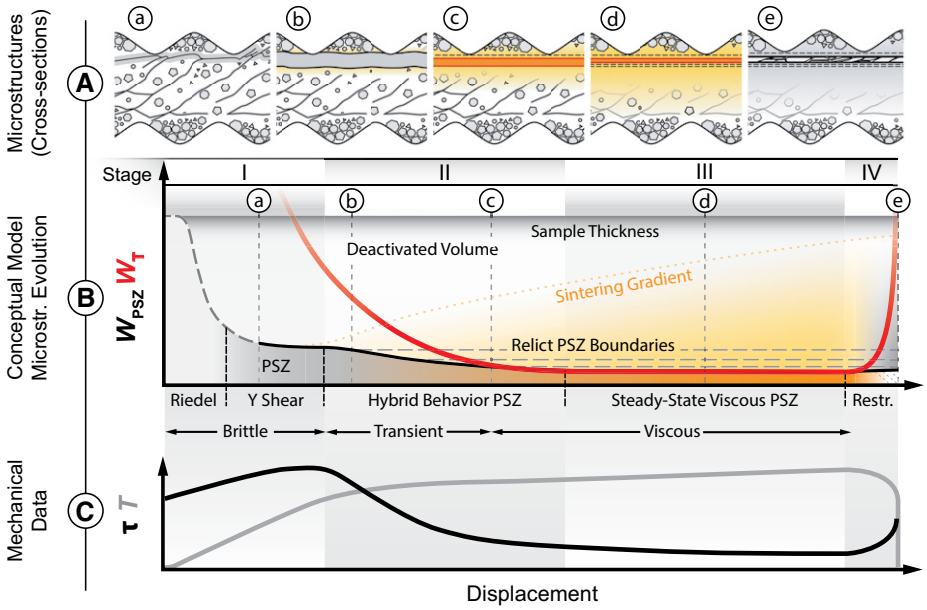


**Figure 4. Graphical representation of the conceptual model with increasing displacement. A: Interpretation of microstructural evolution in the sample. B: Conceptual model comparing the thickness of the actively deforming volume ($W_{PSZ}$; PSZ—principal slip zone) with the theoretical thickness ($W_T$) and evolution of microstructures with increasing displacement. C: Schematics of shear stress (τ) and temperature (*T*) during experiments.**

between the material in the PSZ and that in the SG domains (Fig. 3B). Therefore, the MSs evolve to become strain compatibility boundaries, separating a fine-grained, weak, viscously deforming PSZ (with $\dot{\gamma} > 10^3$), from coarser-grained and sintered volumes. These are passively heated and deform slowly on both sides of the PSZ (also proposed by Smith et al., 2015). If slip (and frictional heating) did localize on the MS, rather than inside the PSZ, the microstructural evidence of the temperature gradient (SG) would be symmetrical with respect to the MS, which it is not (Fig. 3B). MSs are therefore *not* frictional sliding surfaces, as they are commonly interpreted, but instead, they mark sharp rheological contrasts between highly strained (PSZ) and much lower-strained (SG) regions. We interpret that grooves seen on the MSs parallel to slip direction, down to the nanometer scale (Section DR5, Fig. DR7A; De Paola et al., 2015; Smith et. al, 2015), are corrugations of the PSZ boundary. We speculate that they may reflect small local variations in PSZ thickness, in a direction orthogonal to slip; i.e., they are not formed due to abrasive wear. This might be inherited from the irregularity of older MSs (Fig. 3A), formed during Stage II, when the PSZ grain size was less homogeneous (Fig. 2C).

During Stage IV, upon deceleration of the sample to arrest, the PSZ temperature drops, affecting its rheological behavior (Fig. 4C). At this stage, the theoretical thickness is $W_T > W_{PSZ}$ (Fig. 4B). We interpret that the actively deforming PSZ, which is unable to thicken due to its now coarser-grained sintered boundaries, rapidly strengthens and eventually undergoes embrittlement and reworking (Figs. 2D and 2E). Thermal cracking due to fast undercooling and damage during unloading may also enhance the splitting of the sample along preexisting textural discontinuities, such as the MSs, which are then exposed in extracted samples (Section DR5, Fig. DR7A). During the fast (<1 s) cooling stage after the experiments, grain growth due to static recrystallization is very limited, both within and on either side of the PSZ (see De Paola et al., 2015).

## CONCLUSIONS

A simple conceptual model for coseismic weakening in calcite gouges is developed, integrating experimental data, microstructural analysis, and theoretical arguments. We propose that weakening is driven by thermally induced grain-size–sensitive mechanisms active within a PSZ, whose finite thickness is controlled by grain size, temperature, and shear stress.

Careful recovery of the samples has allowed a quantitative characterization of the entire PSZ thickness, which is on the order of a few tens of microns, comparable to the thickness of those found in natural seismic faults in carbonates.

According to our conceptual model, MSs mark rheological contrasts across which an extremely sharp strain gradient is observed. They partition the deformation between the weak, viscously deforming PSZ and the stronger and sintered outer layers. Thus, our observations suggest that MSs are not frictional slip surfaces in the classical sense. Whether their preservation in natural carbonate-hosted fault zones remains indicative of past seismogenic behavior is open to debate. However, seismic slip velocities and coincident shear heating make their formation more likely.


## ACKNOWLEDGMENTS

We thank B.E. Hobbs, S.A.F. Smith, S. Siman-Tov, and an anonymous reviewer for their constructive reviews. This project has received funding from the European Union's Horizon 2020 research and innovation program under the Marie Sklodowska-Curie grant agreement No 642029 - ITN CREEP, and the Natural Environment Research Council (NERC) through a NERC standard grant NE/H021744/1.


## REFERENCES CITED


Barnhoorn, A., Bystricky, M., Burlini, L., and Kunze, K., 2004, The role of recrystallisation on the deformation behaviour of calcite rocks: large strain torsion experiments on Carrara marble: Journal of Structural Geology, v. 26, p. 885–903, https://doi.org/10.1016/j.jsg.2003.11.024.

Bestmann, M., Kunze, K., and Matthews, A., 2000, Evolution of a calcite marble shear zone complex on Thassos Island, Greece: Microstructural and textural fabrics and their kinematic significance: Journal of Structural Geology, v. 22, p. 1789–1807, https://doi.org/10.1016/S0191-8141(00)00112-7.

Collettini, C., Carpenter, B.M., Viti, C., Cruciani, F., Mollo, S., Tesei, T., Trippetta, F., Valoroso, L., and Chiaraluce, L., 2014, Fault structure and slip localization in carbonate-bearing normal faults: An example from the Northern Apennines of Italy: Journal of Structural Geology, v. 67, p. 154–166, https://doi.org/10.1016/j.jsg.2014.07.017.

De Paola, N., Holdsworth, R.E., Viti, C., Collettini, C., and Bullock, R., 2015, Can grain size sensitive flow lubricate faults during the initial stages of earthquake propagation?: Earth and Planetary Science Letters, v. 431, p. 48–58, https://doi.org/10.1016/j.epsl.2015.09.002.

Fondriest, M., Smith, S.A.F., Candela, T., Nielsen, S.B., Mair, K., and Di Toro, G., 2013, Mirror-like faults and power dissipation during earthquakes: Geology, v. 41, p. 1175–1178, https://doi.org/10.1130/G34641.1.

Green, H.W., II, Shi, F., Bozhilov, K., Xia, G., and Reches, Z., 2015, Phase transformation and nanometric flow cause extreme weakening during fault slip: Nature Geoscience, v. 8, p. 484–489, https://doi.org/10.1038/ngeo2436.

Herwegh, M., and Kunze, K., 2002, The influence of nano-scale second-phase particles on deformation of fine grained calcite mylonites: Journal of Structural Geology, v. 24, p. 1463–1478, https://doi.org/10.1016/S0191-8141(01)00144-4.

Hobbs, B., and Ord, A., 2014, Structural Geology: The Mechanics of Deforming Metamorphic Rocks: Amsterdam, Elsevier, 665 p., https://doi.org/10.1016/C2012-0-01215-X.

Poirier, J.-P., 1985, Creep of Crystals: Cambridge, UK, Cambridge University Press, 260 p., https://doi.org/10.1017/CBO9780511564451.

Rice, J.R., 2006, Heating and weakening of faults during earthquake slip: Journal of Geophysical Research: Solid Earth, v. 111, B05311, https://doi.org/10.1029/2005JB004006.

Sammis, C.G., and Ben-Zion, Y., 2008, Mechanics of grain-size reduction in fault zones: Journal of Geophysical Research: Solid Earth, v. 113, B02306, https://doi.org/10.1029/2006JB004892.

Siman-Tov, S., Aharonov, E., Boneh, Y., and Reches, Z., 2015, Fault mirrors along carbonate faults: Formation and destruction during shear experiments: Earth and Planetary Science Letters, v. 430, p. 367–376, https://doi.org/10.1016/j.epsl.2015.08.031.

Siman-Tov, S., Aharonov, E., Sagy, A., and Emmanuel, S., 2013, Nanograins form carbonate fault mirrors: Geology, v. 41, p. 703–706, https://doi.org/10.1130/G34087.1.

Smith, S.A.F., Nielsen, S., and Di Toro, G., 2015, Strain localization and the onset of dynamic weakening in calcite fault gouge: Earth and Planetary Science Letters, v. 413, p. 25–36, https://doi.org/10.1016/j.epsl.2014.12.043.

Smith, S.A.F., Di Toro, G., Kim, S., Ree, J.-H., Nielsen, S., Billi, A., and Spiess, R., 2013, Coseismic recrystallization during shallow earthquake slip: Geology, v. 41, p. 63–66, https://doi.org/10.1130/G33588.1.

Spagnuolo, E., Plümper, O., Violay, M., Cavallo, A., and Di Toro, G., 2015, Fast-moving dislocations trigger flash weakening in carbonate-bearing faults during earthquakes: Scientific Reports, v. 5, p. 1–11, https://doi.org/10.1038/srep16112.

Tesei, T., Collettini, C., Viti, C., and Barchi, M.R., 2013, Fault architecture and deformation mechanisms in exhumed analogues of seismogenic carbonate-bearing thrusts: Journal of Structural Geology, v. 55, p. 167–181, https://doi.org/10.1016/j.jsg.2013.07.007.

Verberne, B.A., Spiers, C.J., Niemeijer, A.R., De Bresser, J.H.P., De Winter, D.A.M., and Plümper, O., 2013, Frictional properties and microstructure of calcite-rich fault gouges sheared at sub-seismic sliding velocities: Pure and Applied Geophysics, v. 171, p. 2617–2640, https://doi.org/10.1007/s00024-013-0760-0.

Yao, L., Ma, S., Platt, J.D., Niemeijer, A.R., and Shimamoto, T., 2016, The crucial role of temperature in high-velocity weakening of faults: Experiments on gouge using host blocks with different thermal conductivities: Geology, v. 44, p. 63–66, https://doi.org/10.1130/G37310.1.



Manuscript received 2 October 2017
Revised manuscript received 23 April 2018
Manuscript accepted 25 April 2018

Printed in USA